Caving 2026 – A van As, D Cumming-Potvin & J Wesseloo (eds)

doi:10.36487/ACG_repo/2645_67

Influence of veining on tensile strength and fragmentation of brittle rock in cave mining

Shakeba Noori [a,*], Cassady Harraden [a], Erik Eberhardt [a], Cajetan Iferobia [a]

[a] *Department of Earth, Ocean and Atmospheric Sciences, The University of British Columbia, Canada*

Abstract

As mining operations target greater depths, the mechanical behaviour of rock masses becomes increasingly complex due to the combined effects of high in situ stresses and the growing dominance of vein networks in low joint intensity rock masses, such as those associated with porphyry deposits. This complexity underscores the importance of orebody knowledge, as the mineralogical and structural characteristics of veining can exert a first-order control on rock mass behaviour and fragmentation processes. While the role of faults and joints has been extensively studied, the influence of veining on rock strength, brittle fracture and fragmentation remains poorly understood. This study examines the impact of vein mineralogy and morphology on the tensile strength and fracture propagation of diorite and skarn using Brazilian tensile strength testing. Veined specimens were tested under controlled laboratory conditions, with fracture propagation monitored using a high-resolution video imaging technique. Fracture responses were classified as crossing, deflecting along the vein–host rock interface or localising along the vein. Vein attributes, including mineralogy and morphology, were shown to exert a strong control on fracture behaviour and tensile strength. In particular, the mechanical contrast between the vein and the host rock played a critical role in fracture development when the dominant vein was oriented at approximately 30° relative to the loading direction. Weak veins preferentially localised fracture propagation, whereas veins with mechanical strength comparable to the host rock were typically crossed by propagating fractures. In contrast, veins that were stronger than the host rock promoted crack deflection or arrest, forcing fractures to propagate through the host rock or along vein–host rock interfaces. Vein and host rock mineralogy are characterised using micro-X-ray fluorescence imaging, shortwave infrared spectroscopy and thin-section petrography. By quantifying how vein properties influence fragmentation behaviour, this research advances understanding of veined rock behaviour and provides insights for geomechanical assessments in deep cave mining environments.

Keywords: *orebody knowledge, veined rock, vein mineralogy, vein geometry, Brazilian tensile strength, brittle fracture behaviour, deep cave mining geomechanics*

1 Introduction

The global demand for critical minerals, particularly copper, continues to rise due to population growth and the transition to clean energy systems. As near-surface copper deposits are depleted and many large open pit mines approach the end of their mine life, the industry is increasingly transitioning towards underground mass mining, particularly block and panel caving for their economic efficiency and capacity for high-tonnage production (Eberhardt 2024). These deeper projects are subject to higher in situ stresses, greater geological uncertainty and more complex caving dynamics, which challenge conventional design methods (Eberhardt et al. 2015).

At such depths, the geomechanical response of massive, competent orebodies is governed by high in situ stresses and the increasing influence of vein networks within low joint intensity rock masses. In these scenarios, conventional rock mass classification schemes, such as the Rock Mass Rating (Bieniawski 1989),

[*] Corresponding author. Email address: Shakeba.noori@eoas.ubc.ca

the Q-system (Barton et al. 1974) and the Geological Strength Index (Hoek et al. 2013), become inadequate because they were developed largely from jointed rock mass case studies in low-stress environments and provide no to limited consideration of veins. Applications of these schemes to massive, veined rock often overlook key differences in cohesion and tensile strength and oversimplify the strength variability associated with different vein types (mineralogy and morphology) and their spatial intensity (Bewick et al. 2022). Veins are geological structures defined as discrete polycrystalline mineral bodies that form within a host rock and are infilled by one or more minerals precipitated from an aqueous solution (Bons 2000). Veins range in length from a few centimetres to hundreds of metres and in thickness from microscopic scales to several metres. Some veins occur as flat, uniformly thick sheets, but more commonly they form lenticular (lens-shaped) or irregular bodies (Best 2003). Veins can be monomineralic or polymineralic and may contain a wide range of minerals (e.g. quartz, calcite, anhydrite, gypsum, sulphides). They typically occur in intersecting sets, producing highly interlocked, angular rock blocks. Because the mineral infill provides cohesion and tensile strength, the veins form stiff boundaries around the blocks, inhibiting block rotation and shear while controlling the strength and mechanical behaviour of the rock mass, further complicating rock mass characterisation (Bewick et al. 2019). The presence of veins can play a controlling role in the caving of competent primary rock, either facilitating or inhibiting gravity-induced fragmentation of the rock mass.

Veins introduce mechanical heterogeneity into the rock mass. They can either strengthen or weaken it, depending on the vein–host strength/stiffness contrast and vein attributes (e.g. orientation, thickness, continuity and mineralogy) (Clark 2020; Clark & Day 2021). This heterogeneity strongly influences both fracturing behaviour and peak strength. Veined rocks typically exhibit lower strength than intact rocks but higher strength than fractured or foliated rocks (Everall & Sanislav 2018; Clark et al. 2019). Veined rocks can be classified based on the strength contrast between the vein material and the host rock (Turichshev 2016). In general, soft-veined rocks localise rupture along the veins, whereas veins stronger than the host rock promote crack deflection or arrest, forcing fractures to propagate through the host rock or along vein–host rock interfaces and increasing the overall mechanical strength of the veined rock (e.g. Virgo et al. 2013; Shang 2020; Kumar & Murthy 2023).

A limited number of studies have investigated the geomechanical response of veined rocks, drawing on mineralogical analyses, field observations, numerical modelling and laboratory experimentation, predominantly under compressive loading conditions. A key advance has been the development of the Composite Geological Strength Index, which aims to better represent hydrothermal veins and stockworks in rock mass strength estimation (e.g. Virgo et al. 2013; Turichshev & Hadjigeorgiou 2015, 2016, 2017; Day 2016; Bewick et al. 2019; Shang 2020; Vergara et al. 2020; Clark & Day 2021; Kumar & Murthy 2023; Ruderham & Day 2023; Xia et al. 2024). Collectively, these studies demonstrate that veins and their characteristics impart a measurable influence on rock mass strength, fragmentation and brittle failure. However, there is still no consensus on how to systematically account for veining in the strength characterisation of massive, low joint intensity rock masses. In particular, tensile strength data for veined rocks remain scarce despite their direct relevance to fragmentation processes, highlighting an important knowledge gap.

In this study, tensile strength is explicitly examined as a fundamental control on brittle rock behaviour, recognising that veins are cohesive features capable of carrying tensile stress. The limited availability of tensile strength data for veined rocks is addressed. Two laboratory methods are commonly used to determine rock tensile strength, namely the direct tensile test and the Brazilian indirect tensile test. In practice, direct tensile testing is rarely performed due to the complexity of specimen preparation and the need for specialised equipment to grip the sample ends. For these reasons, the Brazilian indirect tensile test is more widely applied because it is simpler, more efficient and requires less sample preparation (ASTM International 2023). The method estimates tensile strength by diametrically loading a cylindrical specimen in compression, inducing extension along the loading plane and typically resulting in failure by splitting (Bell 2007).

Against this backdrop, the study investigates the influence of vein mineralogy and morphology on rock tensile strength, fracture pathways and fragmentation using Brazilian tensile testing on veined samples from a deep, porphyry-hosted copper–gold (Cu–Au) cave mining project. The approach integrates detailed pre-experimental geological characterisation with laboratory testing to evaluate how veins of varying mineralogy and morphology influence tensile response. Both veined and non-veined specimens from porphyry and skarn lithologies are tested, enabling direct comparison and improved understanding of how vein characteristics govern fracture propagation and breakage behaviour, with implications for rock mass characterisation and the optimisation of underground mine design and operations.

2 Geological context for testing investigation

A rigorous understanding of orebody geology is fundamental to the design and interpretation of laboratory testing programs, particularly in deep, brittle rock environments where mineralogical and structural features exert a first-order control on mechanical behaviour. In this context, the Deep Mill Level Zone (DMLZ) provides a well-characterised case study that underscores the importance of integrating orebody knowledge into geomechanical investigations. The DMLZ is a major Cu–Au mine located in the East Ertsberg Skarn System within the Grasberg minerals district in Central Papua, Indonesia. The deposit is being mined using panel caving at depths of approximately 1,500 to 1,800 m within a strong, brittle massive to sparsely jointed rock mass. The orebody extends approximately 1,200 m in length and 350 to 500 m in width (Simanjuntak et al. 2020). Mine development initiated in 2008, with production beginning in September 2015. Mining operations are expected to continue until 2041 (Casten et al. 2016). The operation is expected to extract 472 Mt of ore with average grades of 0.87% Cu, 0.71 g/t Au and 4.36 g/t Ag (Budirumantyo et al. 2015; Casten et al. 2016).

From a geomechanical perspective, the significance of the DMLZ lies in the nature of its mineralisation and host rock fabric. Mineralisation occurs as stockwork-style veins hosted in diorite and as disseminated and vein-type mineralisation within skarns developed in sedimentary rocks (Budirumantyo et al. 2015). These features are associated with a multiphase intrusive system dated at 3.28 to 2.97 ± 0.54 Ma (Meirawaty et al. 2018). The geotechnical properties of the dominant lithologies are summarised in Table 1. The diorite comprises a highly competent and massive rock mass with discrete veining that shows limited spatial continuity. Faults are widely spaced, and many are healed or partially healed (Simanjuntak et al. 2020). In such settings, veining represents the primary structural fabric, directly influencing rock strength, fracture propagation and fragmentation behaviour.

Table 1 Representative geotechnical rock mass parameters for Deep Mill Level Zone (data derived from PTFI 2018, as reported by Simanjuntak et al. 2020)

Geotechnical domain	Rock quality designation (%)	Fracture frequency /m	Joint roughness/joint alteration	Uniaxial compressive strength (MPa)	Elastic modulus (GPa)	Poisson's ratio
Diorite	97	1.6	1.6	160	53	0.29
Hornfels	91	2.9	1.5	180	70	0.28
Exoskarn	92	2.4	1.6	135	68	0.25

3 Methodology

Guided by orebody knowledge and the need to ensure that laboratory testing reflects the geological complexity of the deposit, the overall methodological framework integrates advanced pre-experimental geochemical and mineralogical characterisation with mechanical testing. High-resolution imaging and spectroscopic techniques are used in conjunction with conventional thin-section analysis to characterise the mineral composition of veins, alteration halos and host rock. Morphological characterisation is conducted to quantify vein orientation relative to the loading direction, as well as vein and halo thickness.

A series of Brazilian tensile strength (BTS) tests was then performed, in accordance with ASTM standards (ASTM International 2023) and the International Society for Rock Mechanics (ISRM) suggested methods (International Society for Rock Mechanics 1978). The combined dataset was then used to evaluate how vein characteristics, including mineralogy, morphology and intensity, influence tensile strength, fracture propagation pathways and fragmentation behaviour.

3.0 Characterisation methods

State-of-the-art micro-X-ray fluorescence (µXRF) imaging and shortwave infrared (SWIR) spectroscopy were employed to comprehensively characterise the chemistry and mineralogy of veins, halos and host rocks. While µXRF offers high-resolution elemental mapping, it cannot resolve chemically similar minerals or detect light elements (e.g., H, Li, B, C, O). These constraints highlight the value of integrating complementary techniques, such as SWIR spectroscopy for mineral identification and petrographic analysis for mineral confirmation, to better characterise alteration and the mineralogical variability of veins.

3.0.1 Micro-X-ray fluorescence (µXRF)

µXRF analysis was employed to characterise the mineralogy of veins and host rocks, as well as to resolve the spatial distribution of mineral phases within intact core samples prior to preparation of the disc-shaped Brazilian specimens. This non-destructive technique provides high-resolution elemental mapping, enabling identification of veins across a range of thicknesses, including cryptic veins not visible at the drillcore scale. Data were acquired using a Bruker M4 TORNADO spectrometer (Bruker 2024) equipped with a Rh-target X-ray tube. Scanning was conducted under vacuum conditions at 2 mbar, with an excitation voltage of 50 kV and a beam current of 600 µA. A beam size of 20 µm and a dwell time of 10 ms per pixel were used. Four maps were collected per sample, each measuring 12 mm in height and 150–180 mm in width, depending on the core length, with a spatial resolution of 200 µm. Elemental maps were generated for major rock-forming elements (e.g. Ca, Si, Mg, Fe, Na, K) as well as hydrothermal and ore-related elements such as S, Cu, Ti and Zn. These high-resolution datasets facilitated detailed identification of vein–host interactions and mineralogical transitions within alteration halos, providing a basis for linking the mineralogy of the veins, halos and host rocks to rock strength and fragmentation behaviour. The cosine similarity method (CSM) was used to classify mineral phases from quantified µXRF data by comparing the elemental composition of each pixel with reference mineral compositions in a mineral library. CS is a mathematical measure of similarity between two non-zero vectors based on the angle between them (Van der Meer 2006). The mineral phase with the highest CS value was assigned as the best match for each pixel.

3.0.2 Shortwave infrared (SWIR)

SWIR spectroscopy was used to identify hydrothermal alteration minerals in dioritic and skarn rocks. SWIR can distinguish chemically similar alteration minerals such as white micas (e.g. muscovite and phengite), chlorite and epidote, which are often difficult to differentiate using chemical methods alone, such as µXRF. This method is rapid, non-destructive and has minimal sample preparation requirements (Chang & Yang 2012). The oreXpert handheld spectrometer system used in this study operates in the VNIR-SWIR range of 350–2,500 nm and collects spectra from a 3 mm spot. SWIR detects minerals containing hydroxyl groups, water molecules, ammonium ions and carbonates, particularly phyllosilicates and carbonates (Bonner 2020). The collected spectra were analysed to classify mineral phases, and this information was used to further characterise the phyllosilicate and carbonate mineralogy, enhancing the mineralogical characterisation of veins and host rock.

3.0.3 Thin-section petrography

Thin-section petrography was used to validate and refine interpretations from µXRF and SWIR analyses, ensuring accurate vein mineralogy and host rock characterisation. Polished thin sections were prepared for microscopic analysis to examine grain size, shape and fabric, as well as textural relationships between veins, alteration halos and the surrounding host rock.

3.1 Tensile strength testing

3.1.1 Sample preparation

A total of nine disc-shaped specimens, comprising both veined and non-veined diorite and exoskarn, were selected from multiple drillholes. Sample selection was guided by orebody knowledge to capture representative variations in lithology, vein density, mineralogy and degree of hydrothermal alteration. The specimens were prepared according to ASTM International (2023) by precision cutting and grinding to produce flat, parallel disc geometries suitable for Brazilian tensile testing. Two specimen diameters were used, 63 and 47 mm, with thicknesses selected to achieve slenderness ratios (t/D) between 0.2 and 0.75, consistent with recommended testing standards (ASTM International 2023). Detailed pre-test characterisation, including specimen dimensions, lithology and veining attributes, is summarised in Table 2.

Table 2 Summary of specimen specifications, including dimensions and lithology

	Sample ID	Diameter (D) (mm)	Thickness (t) (mm)	t:D ratio	Rock type/alteration	Vein count
1	DZ30-N1F-1101-72.40	63	34	0.54	Diorite (propylitic)	1
2	DZ26-10EF-02-69.65	63	30.05	0.48	Diorite (propylitic)	1
3	DZ30-N1F-1101-343.40-343.60	54	45	0.83	Exoskarn	2
4	DZ30-N2F-0301-306.20-306.40	47	28	0.60	Diorite (propylitic)	–
5	DZ26-10EF-02-74.45	63	32	0.51	Diorite (propylitic)	2
6	DZ30-N2F-0301-260.80-261	47	28	0.60	Diorite (propylitic)	3
7	DZ30-N1F-1101-251.50-251.70	63	43	0.68	Diopside–anhydrite exoskarn	3
8	DZ30-N1F-1101-252-252.20	63	31	0.49	Diopside–anhydrite exoskarn	4
9	DZ30-N1F-1101-342.30-342.50	63	33	0.52	Diorite (propylitic-endoskarn)	7

3.1.2 Testing set-up

The Brazilian test was conducted by applying a concentrated compressive load diametrically along the centre of the disc-shaped specimens using curved jaw platens. The thickness of the samples and the loading rate were selected in accordance with ASTM International (2023), while the curved jaw platen configuration aligns with the ISRM (1978) suggested methods. All tests were performed at The University of British Columbia using a servo-controlled, stiff loading frame. An axial load rate of 6 kN/min was selected to ensure specimen failure within 1–10 minutes, as recommended by ASTM International (2023). Veined specimens were loaded diametrically with dominant vein orientations inclined 30° relative to the loading direction until failure. This orientation was selected as it approximates the critical angle at which tensile stresses at flaw tips are maximised, with the vein acting as the flaw, thereby competing with the diametrical tensile stress expected in a homogeneous specimen in promoting crack initiation and propagation (Eberhardt et al. 2016).

Tensile strength was determined indirectly under the assumption that the applied compressive load induces a uniform tensile stress along the vertical diameter of the disc, resulting in tensile crack initiation at the specimen centre. During testing, fracture propagation was visually observed and documented using a high-resolution (4K) camera operating at 60 frames per second. Particular attention was given to the interaction between developing fractures and veins of differing mineralogy, thickness, position and orientation, relative to the loading direction.

The maximum compressive axial load recorded at failure is then used to calculate the tensile strength using the following relationship recommended by ASTM International (2023) and ISRM (1978):

$$\sigma_t = \frac{2P}{\pi D t} \tag{1}$$

where:

σ_t	=	tensile strength
P	=	maximum axial load at failure
D	=	diameter of the disc
t	=	thickness of the specimen.

4 Results

4.0 Micro-X-ray fluorescence characterisation of vein attributes

High-resolution µXRF elemental mapping enabled the identification of veins of varying thickness and mineralogy, associated alteration halos and host rock mineralogy in the analysed diorite and skarn samples. Although µXRF provides elemental rather than mineralogical maps, the application of the CSM allowed for robust mineralogical interpretation and effective mapping of the veined samples. The µXRF analyses were conducted on the surfaces of the intact core samples selected for later triaxial testing, which will be undertaken in a second phase of this study to evaluate the influence of confinement on crack initiation and propagation as a function of veining intensity. The BTS specimens were prepared from the ends of these triaxial cores, with the resulting mineralogical information used to infer the mineralogy of the diametrically cut BTS test surfaces. Representative mineralogical maps from this analysis are presented in Figure 1.

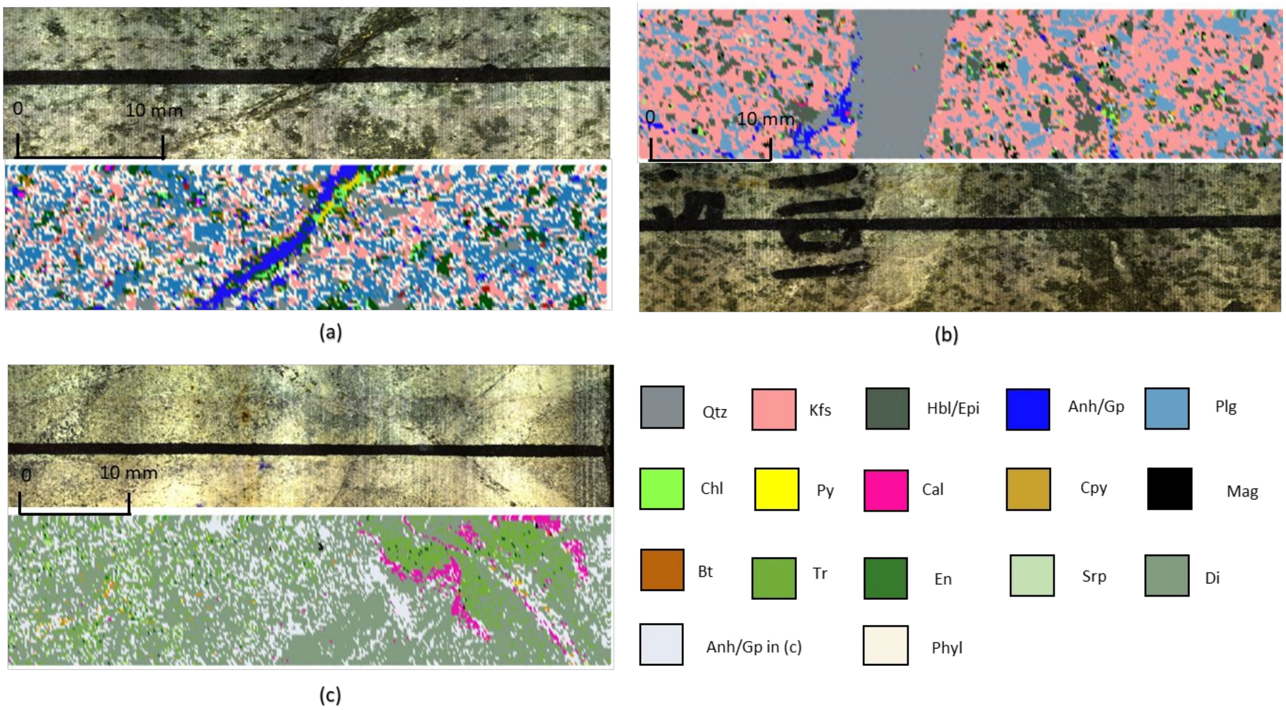

Figure 1 Micro-X-ray fluorescence-derived mineralogy calculated using the cosine similarity method (CSM) for three representative samples: (a) DZ30-N2F-0301-260.80–261.00; (b) DZ30-N1F-1101-342.30–342.50; and (c) DZ30-N1F-1101-251.50–251.70 (Abbreviations: Anh = anhydrite; Bt = biotite; Chl = chlorite; Cal = calcite; Cpy = chalcopyrite; Di = diopside; En = enstatite; Epi = epidote; Gp - gypsum; Hbl - hornblende; Kfs - K-feldspar; Mag - magnetite; Plg - plagioclase; Py - pyrite; Phyl - phyllosilicates; Qtz - quartz; Srp - serpentine; Tr - tremolite)

4.1 Shortwave infrared analysis results

SWIR spectroscopy was conducted to characterise the alteration mineralogy of diorite and skarn samples, providing a broad assessment rather than focusing on specific veins or halos. The results highlight distinct alteration minerals in each rock type, reflecting hydrothermal and metasomatic processes. A detailed breakdown of the identified mineral groups and types for the samples is presented in Table 3. These SWIR-identified minerals were used to construct the reference mineral library employed in the CSM for mineralogical interpretation of the µXRF elemental maps.

Table 3 Summary of alteration minerals (hydrous and hydroxyl-bearing phases) identified by shortwave infrared (SWIR) spectroscopy for the samples analysed in this study

Sample ID	Rock type	SWIR-identified minerals
DZ30-N1F-1101-72.40	Diorite (Prop)	Hbl, Chl, Sd, Mnt, Dol
DZ26-10EF-02-69.65	Diorite (Prop)	Hbl, Chl, Gyp/Anh
DZ30-N1F-1101-343.40–343.60	Exoskarn	Hbl, Phl, Chl, Ms, Ill
DZ30-N2F-0301-306.20–306.40	Diorite (Prop)	Chl, Ank, Mnt
DZ26-10EF-02-74.45	Diorite (Prop)	Phl, Gyp, Ms–Phg
DZ30-N2F-0301-260.80–261.00	Diorite (Prop)	Chl, Mnt, Ank
DZ30-N1F-1101-251.50–251.70	Di–Anh exoskarn	Tr, Srp
DZ30-N1F-1101-252.00–252.20	Di–Anh exoskarn	Tr, Srp, Chl
DZ30-N1F-1101-342.30–342.50	Diorite (Prop–Endo)	Hbl, Chl, Ank, Ms

Abbreviations: Ank–ankerite; Anh–anhydrite; Chl–chlorite; Di–diopside; Dol–dolomite; Gyp–gypsum; Hbl–hornblende; Ill–illite; Mnt–montmorillonite; Ms–muscovite; Phg–phengite; Phl–phlogopite; Prop–propylitic alteration; Endo–endoskarn; Sd–siderite; Srp–serpentine; Tr–tremolite

4.2 Thin-section analysis

Thin-section petrography confirms the mineralogy and vein–host relationships identified through µXRF and SWIR. An example from sample DZ30 N1F 1101 342.30–342.50 (Figure 2) shows an anhydrite–quartz–sulphides vein cutting altered feldspar–hornblende host rock, which contains minor quartz, magnetite and sulphide minerals.

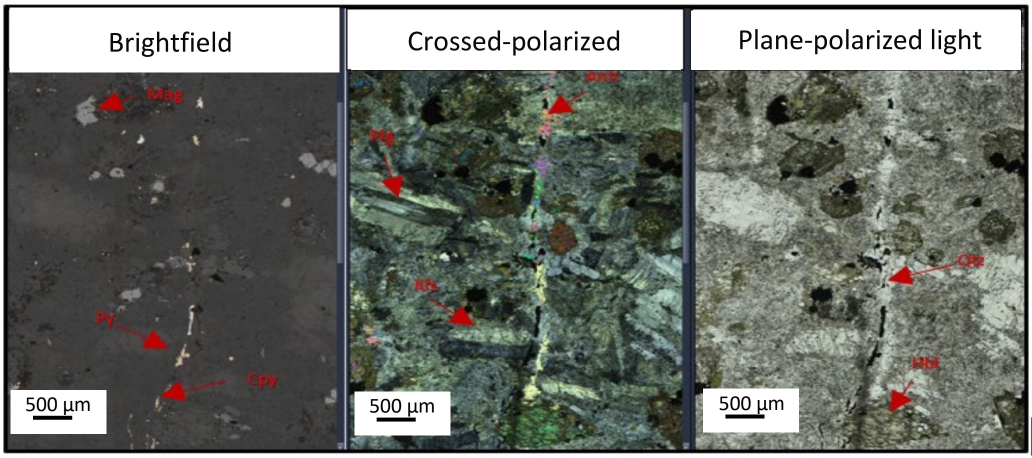

Figure 2 Representative thin-section photomicrographs of altered diorite under reflected/brightfield microscopy, cross-polarised light, and plane-polarised light (Abbreviations: Anh–anhydrite; Cpy–chalcopyrite; Kfs–K-feldspar; Hbl–hornblende; Mag–magnetite; Py–pyrite; Qtz–quartz; Plg–plagioclase)

4.3 Brazilian test results

BTS testing indicates that the presence of veins affected both the measured tensile strength and the associated fracture-propagation behaviour. Due to the limited availability of intact, non-veined specimens across all lithologies and specimen diameter sizes, systematic comparison was not possible for every case. However, for the 47 mm diameter diorite specimens, the veined sample exhibited higher tensile strength (16.3 MPa) than the intact specimens (14.9 MPa). This increase may be attributed to the presence of a feldspar–anhydrite vein along which fracture propagation was partially localised within the anhydrite portion (Figure 5; Table 4). Given the limited dataset, this observation should be interpreted cautiously.

Across all tested specimens, tensile strengths were broadly comparable between diorite and exoskarn specimen lithologies, except one veined exoskarn sample (DZ30-N1F-1101-252.0–252.20) containing diopside–anhydrite veins, which exhibited the highest tensile strength and failed after a substantially longer loading duration, indicating a greater resistance to tensile failure. A summary of all results, spanning a range of vein mineralogies and geometries, is presented in Table 4.

Fracture propagation behaviour varied systematically with vein characteristics. In specimens containing veins composed of minerals weaker than the host rock, fractures preferentially propagated along the vein plane. Where vein minerals had mechanical properties comparable to the host rock, fractures typically crossed the vein with minimal deflection. In contrast, veins composed of stronger minerals promoted fracture deflection along the vein–host interface or remained largely intact during failure. Representative fracture patterns for all tested specimens are shown in Figure 3-11.

5 Discussion

The results demonstrate that fracture propagation during Brazilian tensile testing is strongly governed by contrasts in mechanical properties between veins and the host rock, as well as by vein geometry and position relative to the applied stress field. Veins composed of mechanically weaker minerals act as preferential fracture pathways, promoting fracture localisation. This behaviour is consistent with observations from compressive loading studies (e.g. Shang 2020; Kumar & Murthy 2023) and with numerical modelling of vein–extension fracture interactions by Virgo et al. (2013). For example, in sample DZ26-10EF-02-69.65, a biotite micro-vein oriented at 30° localised fracture propagation relative to the stronger host rock (Figure 9; Table 4), confirming that vein-controlled weakening mechanisms also operate under indirect tensile loading.

Where vein and host rock properties are comparable, veins exert limited influence on fracture development. In such cases, fractures propagate across veins in a similar manner to intact host rock behaviour, in agreement with the numerical modelling results of Virgo et al. (2013). This is evident in the diopside–anhydrite exoskarn specimens (Figure 6, 10; Table 4) and in diorite samples (Figure 8; Table 4), where veins composed of minerals with comparable hardness and strength to the host rock (feldspar, hornblende, quartz and anhydrite) did not significantly alter fracture trajectories.

In contrast, mechanically stronger veins act as barriers to fracture propagation, promoting deflection along vein–host rock interfaces or limiting fracture participation altogether. This behaviour is consistent with previous observations by Virgo et al. (2013) and Shang (2020). For example, in sample DZ30-N1F-1101-343.40-343.60, a quartz vein within a diopside–anhydrite exoskarn host inhibited fracture propagation across the vein and promoted fracture localisation along the vein–host interface due to its higher strength relative to the surrounding rock (Figure 11; Table 4). Similarly, in sample DZ30-N1F-1101-342.30–342.50, a dominant quartz–anhydrite vein ($\alpha = 30°$, $t = 6.5$ mm), surrounded by hornblende ± epidote ± chlorite ± chalcopyrite halos (halo $t < 1$ mm), is oriented such that it lies within the central tensile stress field during loading. In this case, fractures propagated across and partially localised within the weaker anhydrite portion of the vein. At the same time, the quartz segment remained intact, effectively inhibiting continuous fracture localisation along the full vein length (Figure 8, Table 4).

Table 4 Summary of Brazilian tensile test results for the tested specimens, including tensile strength and fracture pattern

Sample ID	Rock type (alteration)	Vein count and mineralogy	Vein thickness, t (mm)	Vein orientation, α (°)*	Tensile strength, σ_t (MPa)	Fracture pattern
DZ30-N1F-1101-72.40	Diorite (Prop)	1 vein: Bt + Chl haloed by Kfs + Qtz	$Vt_1 < 1$	55°, off centre	12.2	Crossed
DZ26-10EF-02-69.65	Diorite (Prop)	1 vein: Bt	$Vt_1 \ll 1$	30°	12.6	Completely localised along vein
DZ30-N1F-1101-343.40–343.60	Exoskarn	2 veins: V1–V2 Qtz ± Cpy	$Vt_1 = 9$; $Vt_2 = 2$	5°, subparallel	7.5	Propagated along the vein–host interface
DZ30-N2F-0301-306.20–306.40	Diorite (Prop)	Intact (non-veined)	n/a	n/a	14.9	Intact-like splitting
DZ26-10EF-02-74.45	Diorite (Prop)	2 veins: V1 Cpy + Fsp + Anh + Qtz; V2 Hbl + Bt	$Vt_1 = 1$; $Vt_2 < 1$	V1 = 30°	11.4	Primary fracture crossed V1
DZ30-N2F-0301-260.80–261.00	Diorite (Prop)	3 veins: Anh + Feldspar, Bt±Chl±Hbl/Epi halos	Veins < 1; halos < 1	–	16.3	Crossed, partially localised along Anh portion of vein 1
DZ30-N1F-1101-251.50–251.70	Di-Anh exoskarn	3 veins: Di + Anh + Cal; halo Di + Tr	$Vt_1 < 1$; $V_{t2} = 1$; $V_{t3} < 1$; halo = 5	V3 = 30°	11.6	Crossed host rock with minor deflection
DZ30-N1F-1101-252.00–252.20	Di-Anh exoskarn	4 veins: V1–V2 Anh + Di ± Cal; V3–V4 Di	All t < 1	V2 = 30°	22.5	Multiple fractures crossing veins
DZ30-N1F-1101-342.30–342.50	Diorite (Prop–Endo)	7 veins: V1-5 Hbl ± Ep ± Chl; V6 Kfs + Anh + Hbl; V7 Qtz + Anh, Hbl ± Ep ± Chl ± Cpyhalo	Vt_1–6 < 1; Vt_7 = 6.5 (dominant)	V7 = 30°	11.1	Crossed and partially localised along Anh in V7

Abbreviations: Anh–anhydrite; Bt–biotite; Cal–calcite; Chl–chlorite; Cpy–chalcopyrite; Di–diopside; Epi–epidote; Endo–endoskarn; Fsp–feldspar; Hbl–hornblende; Kfs–K-feldspar; Prop–propylitic alteration; Qtz–quartz; Tr–tremolite; σ_t–tensile strength

*Vein orientation (α) is measured relative to the applied diametral loading direction

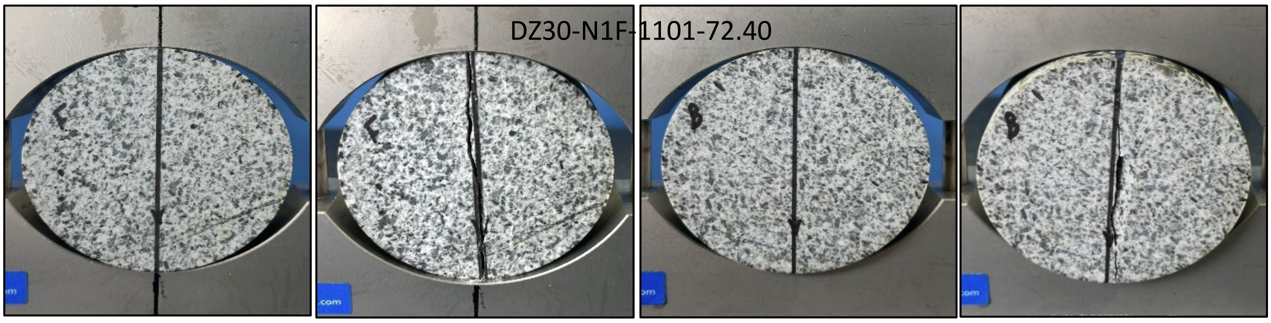

Figure 3 **Specimens showing, from left to right, front (F) and back (B) views before and after testing, illustrating fracture propagation during tensile loading and the influence of vein mineralogy, orientation and thickness on fracture pathways and failure behaviour. Here, α denotes the vein angle relative to the loading direction, and t denotes vein thickness. Fracture crosses a feldspar–hornblende vein (α = 55°, t < 1 mm) where vein strength is comparable to the host rock**

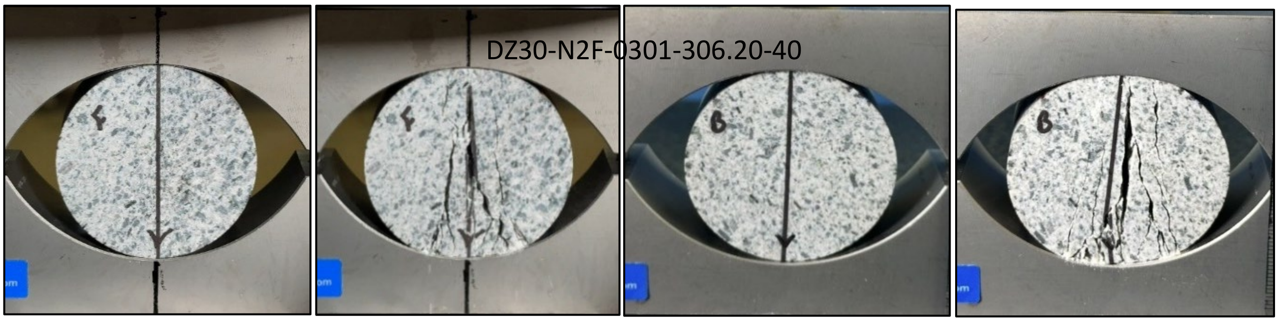

Figure 4 **Multiple tensile fractures in an intact, non-veined specimen**

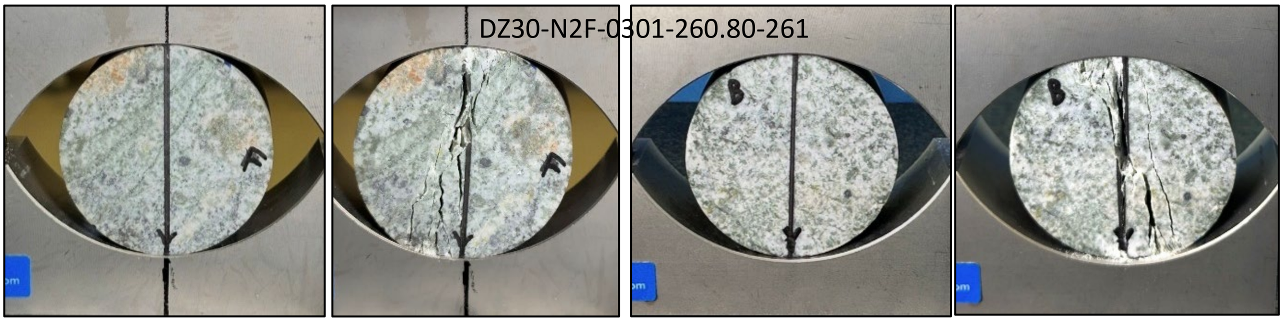

Figure 5 **Fracture partially localising along the anhydrite portion of the vein before propagating into the host rock**

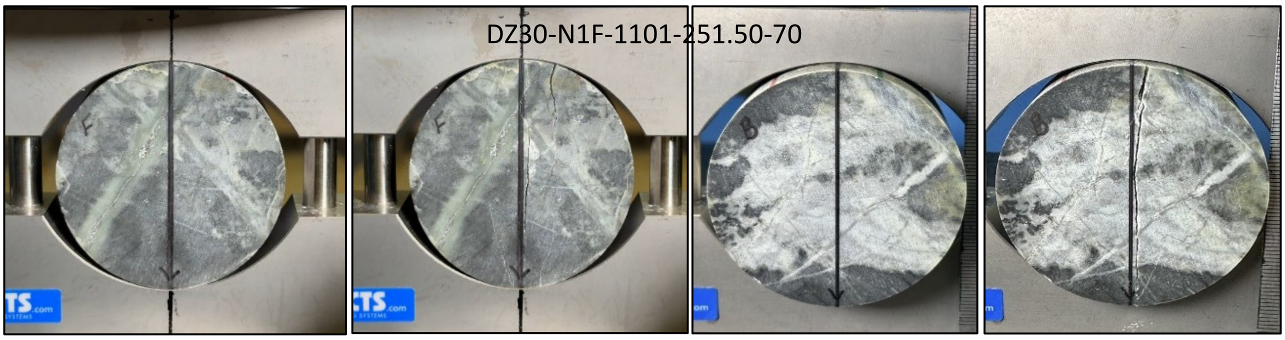

Figure 6 **Splitting fracture formed through the specimen centre, crossing diopside–anhydrite–calcite veins, exhibiting behaviour comparable to a non-veined counterpart**

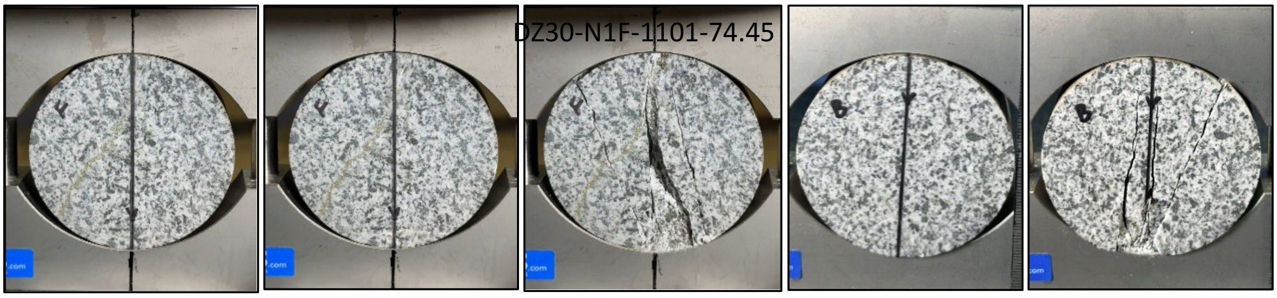

Figure 7 Primary fracture initiated from the left edge and crossing a chalcopyrite–feldspar–anhydrite vein (second figure from the left), while a secondary fracture formed at the centre and partially localised along the anhydrite portion of the vein

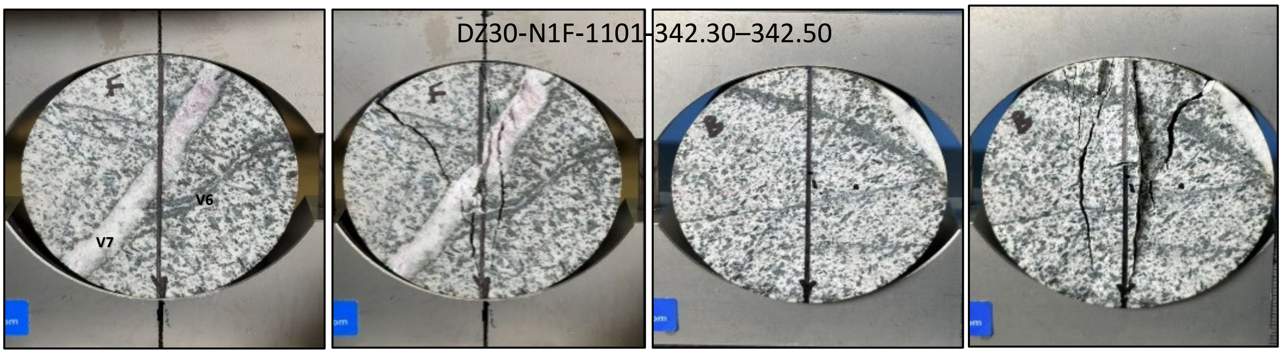

Figure 8 Fracture initiated at the centre and crosses the vein, with secondary fractures intersecting V6 and V7 and locally deflecting along the upper edge of the anhydrite portion (upper right), while no fracture develops within the quartz portion (lower left); where veins are composed of hornblende ± anhydrite ± feldspar, fractures cross the veins similarly to the host rock

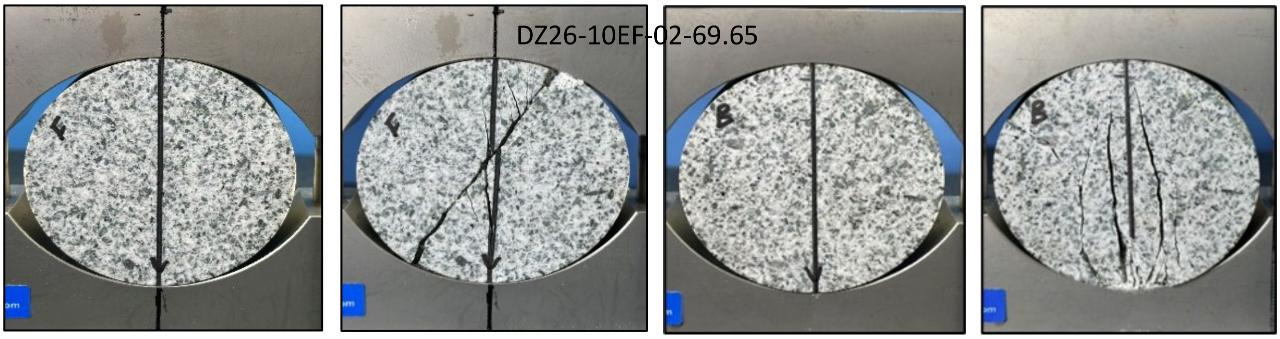

Figure 9 Fracture propagating along a biotite micro-vein (α = 30°, vein weaker than host rock)

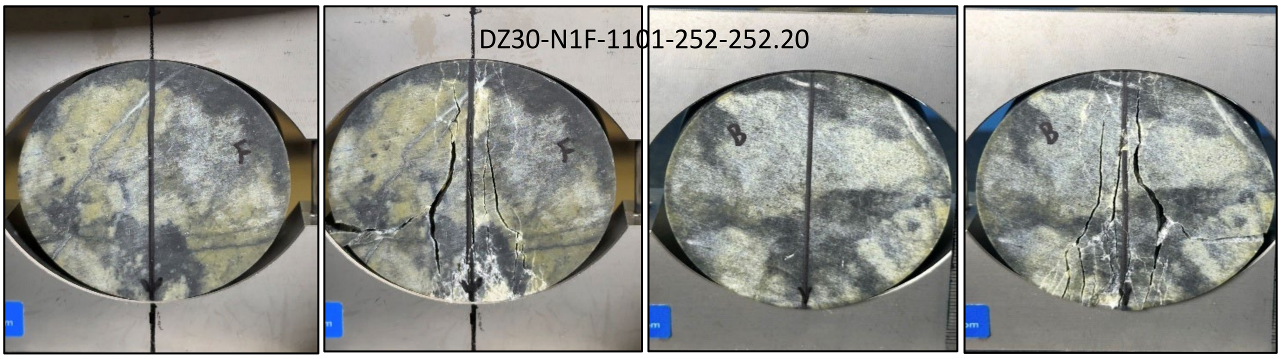

Figure 10 Fractures crossing diopside–anhydrite veins haloed by diopside ± tremolite; involves vein strength comparable to that of the exoskarn host rock

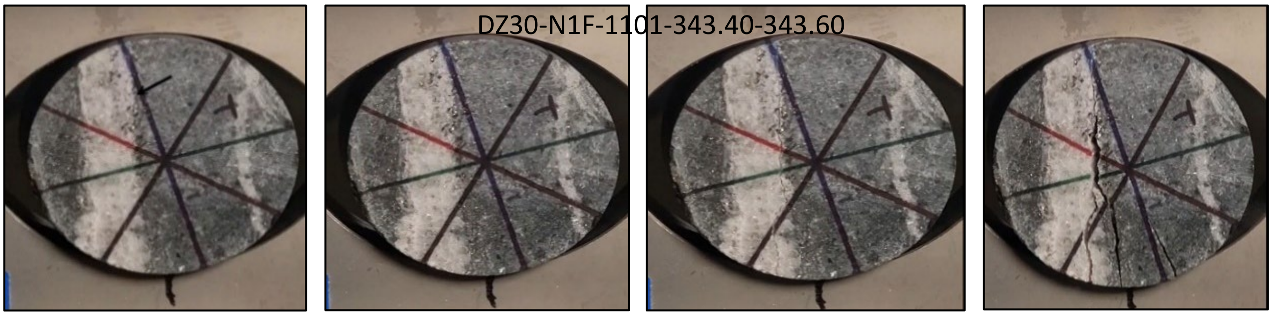

Figure 11 Fracture propagating along the vein and host rock interface, where the vein was stronger than the host rock (quartz; Mohs hardness = 7), and is subparallel to the loading

It was also observed that the position of veins relative to the loading direction plays a crucial role in controlling fracture processes during Brazilian tensile testing. Veins located outside the central tensile stress region did not contribute to fracture initiation or propagation.

Veins oriented at approximately 30° to the loading direction and intersecting the region of maximum tensile stress were consistently involved in the fracture process, indicating that this orientation represents a critical configuration for crack initiation and propagation under indirect tensile loading conditions, with even micro-scale veins (t<1 mm) participating where they are mechanically weaker than the host rock.

In a cave mine design context, these results highlight that the tensile behaviour of veined rock and its control on fracture propagation and fragmentation should not be treated as secondary effects or simplified as uniformly weak discontinuities. Rather, vein mineralogy strength contrast relative to the host rock, geometry and intensity exert a first-order influence on crack initiation, propagation and fragmentation behaviour. This has direct implications for geomechanical characterisation and design, including the selection of Hoek–Brown parameters, estimates of intact rock strength and disturbance factors. From both primary and secondary fragmentation perspectives, mechanically weaker veins may promote fracture localisation and finer fragmentation. In contrast, stronger veins may inhibit crack growth, contributing to coarser fragmentation or massive rock behaviour and associated high stress hazards such as strainbursting (see Roy et al. 2023). Veins with properties similar to the host rock tend to have limited influence and behave comparably to intact material.

These findings reinforce the need for orebody characterisation approaches that explicitly incorporate vein attributes and associated mechanical contrasts into rock mass characterisation models and fragmentation assessments, providing a more robust basis for predicting caving performance, managing geohazards, and optimising cave design and draw strategies.

6 Conclusion

This study integrated advanced pre-experimental mineralogical and geochemical characterisation with BTS testing to investigate the influence of vein mineralogy and morphology on tensile strength, fracture propagation and fragmentation behaviour in veined diorite and exoskarn samples from the DMLZ panel cave mine. High-resolution micro-X-ray fluorescence elemental mapping interpreted using the CSM, together with shortwave infrared spectroscopy and thin-section petrography, enabled detailed characterisation of veins, alteration halos and host rock mineralogy before mechanical testing.

The results demonstrate that mechanical contrasts between veins and the host rock exert a first-order control on fracture propagation under indirect tensile loading. Veins composed of mechanically weaker minerals relative to the host rock promoted fracture localisation. They acted as preferential fracture pathways, whereas veins with mineralogy and mechanical properties comparable to those of the host rock do not significantly impede fracture growth, even where vein orientation is near-critical (30°), and thickness varies. In contrast, strong quartz-rich veins acted as mechanical barriers, promoting fracture deflection along vein–host rock interfaces or locally inhibiting fracture propagation.

Vein position and orientation relative to the applied loading were also shown to be critical. Veins intersecting the central tensile stress zone and oriented at approximately 30° to the loading direction consistently participated in fracture initiation and propagation, whereas veins located outside this zone exerted a negligible influence on the failure process. These observations underscore the importance of considering both mineralogical contrasts and geometrical characteristics when assessing tensile failure mechanisms in veined rock masses.

Overall, the study demonstrates that vein mineralogy, mechanical contrasts, geometry and position relative to the tensile stress field govern both brittle fracture propagation and fragmentation potential in veined rock. Veins that are mechanically weaker than the host rock promote fracture localisation and finer fragmentation, whereas stronger quartz-rich veins can arrest or deflect fractures, favouring coarser fragmentation and more massive rock behaviour. These results support the inclusion of vein attributes in rock mass characterisation and fragmentation assessment frameworks used to evaluate caveability, drawpoint performance and brittle failure potential. Although the findings are constrained by the limited number of intact, non-veined reference specimens, narrow vein thickness range, limited orientation variation and overall sample size, they provide a clear basis for future work. Expanded testing across lithologies, vein geometries, thicknesses and orientations, combined with uniaxial and triaxial compression testing, will place the observed tensile behaviour within representative deep caving stress paths and improve predictive models of fracture propagation and rock fragmentation.

Acknowledgement

The authors gratefully acknowledge PT Freeport Indonesia and the DMLZ for providing the rock samples and associated data used in this study. Special thanks are extended to Dr Justin Roy for his guidance in initiating the work, Ryan Campbell for his continued support throughout the project, and Dr Shaun Barker and the Mineral Deposit Research Unit for providing access to laboratory facilities and equipment used in the micro-XRF and SWIR analyses. Funding support that made this research possible was provided by PT Freeport Indonesia, the Centre for Innovation in Mineral Resource Engineering, Mitacs and the Natural Sciences and Engineering Research Council of Canada.

References

ASTM International 2023, ‘ASTM D3967-23: Standard test method for splitting tensile strength of intact rock core specimens with flat loading platens’, ASTM International.

Barton, N, Lien, R & Lunde, J 1974, ‘Engineering classification of rock masses for the design of tunnel support’, *Rock Mechanics*, vol. 6, pp. 189–236.

Bell, FG 2007, ‘Rock properties and their assessment’, *Engineering geology*, 2nd edn, Butterworth-Heinemann (Elsevier), Oxford.

Best, MG 2003, *Igneous and metamorphic petrology*, 2nd edn, Blackwell Science Ltd.

Bewick, R, Brzovic, A, Rogers, S, Griffiths, C & Otto, SA 2022, 'Benchmarking framework for porphyry copper-gold rock masses for caveability and fragmentation decision-making', in Y Potvin (ed.), *Caving 2022: Proceedings of the Fifth International Conference on Block and Sublevel Caving*, Australian Centre for Geomechanics, Perth, pp. 1303–1318, https://doi.org/10.36487/ACG_repo/2205_91

Bewick, RP, Kaiser, PK & Amann, F2019, ‘Strength of massive to moderately jointed hard rock masses’, *Journal of Rock Mechanics and Geotechnical Engineering*, vol. 11, 562–575.

Bieniawski, Z 1989, Engineering rock mass classifications: A complete manual for engineers and geologists in mining, civil, and petroleum, Wiley Interscience, Toronto.

Bonner, EP 2020, *Shortwave infrared spectral analysis of hydrothermal alteration in the Main and Southwest Tintic Mining District and exploration implications of the Silver City porphyry Cu-Mo-Au prospect, Tintic Mining District, Utah, USA*, master’s thesis, Colorado School of Mines, Golden.

Bons, PD 2000, ‘The formation of veins and their microstructures’, *Journal of the Virtual Explorer*, vol. 2, p. 12.

Bruker 2026, 'Rock characterization for mineral exploration', Bruker Analytics, Billerica, https://www.bruker.com/en/applications/minerals-mining-and-petrochemical/minerals-exploration-discovery/rock-characterization-for-mineral-exploration.html

Budirumantyo, Silalahi, P, Meiriyanto, F, Antoro, B, Sunyoto, W, Soebari, L, Jong, G, Wibowo, EA & Siahaan, MR 2015, ‘Deep Mill Level Zone (DMLZ) of East Ertsberg Skarn System (EESS), Papua; geology factors of disking core in DMLZ mine’, in *Prosiding TPT XXIV dan Kongres IX Perhapi* [Proceedings of the 24th Annual Technical Meeting and 9th Congress of PERHAPI], 90–98.

Casten, T, Priatna, A & Rumbino, H 2016, 'Deep Mill Level Zone—from feasibility to production', *MassMin 2016: Seventh International Conference and Exhibition on Mass Mining*, Carlton.

Chang, Z & Yang, Z 2012, 'Evaluation of inter-instrument variations among short wavelength infrared (SWIR) devices', *Economic Geology*, vol. 107, no. 7, pp. 1479–1488.

Clark, MD 2020, *Geomechanics and mineralogical characterization of intact heterogeneous rocks from the Legacy Skarn Deposit*, master's thesis, Queen's University.

Clark, MD & Day, JJ 2021, 'Mineralogical and sample selection implications for geomechanical properties of intact heterogeneous and veined rocks from the Legacy skarn deposit', *Engineering Geology*, vol. 285.

Clark, MD, Day, JJ & Diederichs, MS 2019, 'Assessing the geomechanical behaviours of skarn related hydrothermal veins in intact laboratory tests', *Proceedings of the 53rd US Rock Mechanics/Geomechanics Symposium*, American Rock Mechanics Association, Alexandria.

Day, JJ 2016, *The influence of healed intrablock rockmass structure on the behaviour of deep excavations in complex rockmasses*, PhD thesis, Queen's University, Kingston.

Eberhardt, E 2024, 'The copper supply gap: Mining bigger and deeper', in PD Tortell (ed.), *Heavy metal: Earth's minerals and the future of sustainable societies*, Open Book Publishers, Cambridge, pp. 171–179.

Eberhardt, E, Diederichs, MS & Rahjoo, M 2016, 'Pre-peak brittle fracture damage', in X-T Feng (ed.), Rock mechanics and engineering, Volume 1: Principles, CRC Press, Leiden, pp. 623–657.

Eberhardt, E, Woo, K, Stead, D & Elmo, D 2015, 'Transitioning from open pit to underground mass mining: Meeting the rock engineering challenges of going deeper', *Proceedings of the 13th International Congress of Rock Mechanics: Innovations in Applied and Theoretical Rock Mechanics*, International Society for Rock Mechanics, Lisbon, pp. 1–14.

Everall, TJ & Sanislav, IV 2018, 'The influence of pre-existing deformation and alteration textures on rock strength, failure modes and shear strength parameters', *Geosciences*, vol. 8, no. 4, 124.

Hoek, E, Carter, TG & Diederichs, MS 2013, 'Quantification of the Geological Strength Index chart' *Proceedings of the 47th US Rock Mechanics/Geomechanics Symposium*, American Rock Mechanics Association, Alexandria. pp. 1–8.

International Society for Rock Mechanics 1978, 'Suggested methods for determining tensile strength of rock materials', International *Journal of Rock Mechanics and Mining Sciences and Geomechanics Abstracts*, vol. 15, no. 3, pp. 99–103.

Kumar, D & Murthy, PSK 2023, 'Influence of calcite veins on the failure mode and mechanical behaviour of basalt', *Proceedings of the International Conference on Trends and Recent Advances in Civil Engineering (TRACE 2022)*, Springer Nature, Singapore, pp. 419–427.

Meirawaty, M, Furqan, RA, Nuryana, SD & Yani, A 2018, 'The alteration characteristic of Cu–Au skarn and porphyry style alteration in the Deep MLZ, Ertsberg District, Papua, Indonesia', IOP Conference Series: Earth and Environmental Science, vol. 212, no. 1.

Roy, JM, Eberhardt, E, Bewick, RP & Campbell, R 2023, 'Application of data analysis techniques to identify rockburst mechanisms, triggers, and contributing factors in cave mining', *Rock Mechanics and Rock Engineering*, vol. 56, no. 4, pp. 2967–3002.

Rudderham, GA & Day, JJ 2023, 'Veined rock performance under uniaxial and triaxial compression using calibrated finite element numerical models', *Geotechnics*, vol. 3, no. 4, pp. 1219–1250.

Shang, J 2020, 'Rupture of veined granite in polyaxial compression: Insights from three-dimensional discrete element method modeling', *Journal of Geophysical Research: Solid Earth*, vol. 125.

Simanjuntak, K, Primadiansyah, A, Soumilena, N & Teweng, W 2020, 'Driving and managing stress in the Deep Mill Level Zone caving mine', in R Castro, F Báez & K Suzuki (eds), *MassMin 2020: Proceedings of the Eighth International Conference & Exhibition on Mass Mining*, University of Chile, Santiago, pp. 394–405, https://doi.org/10.36487/ACG_repo/2063_25

Turichshev, A 2016, *Experimental and numerical investigations of the behaviour of intact veined andesite*, PhD thesis, University of Toronto, Toronto.

Turichshev, A & Hadjigeorgiou, J 2015, 'Experimental and numerical investigations into the strength of intact veined rock', *Rock Mechanics and Rock Engineering*, vol. 48, pp. 1897–1912.

Turichshev, A & Hadjigeorgiou, J 2016, 'Triaxial compression experiments on intact veined andesite', *International Journal of Rock Mechanics and Mining Sciences*, vol. 86, pp. 179–193.

Turichshev, A & Hadjigeorgiou, J 2017, 'Quantifying the effects of vein mineralogy, thickness, and orientation on the strength of intact veined rock', *Engineering Geology*, vol. 226, pp. 199–207.

Van der Meer, F 2006, 'The effectiveness of spectral similarity measures for the analysis of hyperspectral imagery', *International Journal of Applied Earth Observation and Geoinformation*, vol. 8, no. 1, pp. 3–17.

Vergara, MR, Arismendy, A, Libreros, A & Brzovic, A 2020, 'Numerical investigation into strength and deformability of veined rock mass', *International Journal of Rock Mechanics and Mining Sciences*, vol. 135, 104510.

Virgo, S, Abe, S & Urai, JL 2013, 'Extension fracture propagation in rocks with veins: Insight into the crack seal process using discrete element method modeling', *Journal of Geophysical Research: Solid Earth*, vol. 118, no. 10, pp. 5236–5251.

Xia, Y, Xu, DP, Jiang, Q, Xie, J & Li, Z 2024, 'The effect of pegmatite veins on fracture behaviours of granite in a deep large underground cavern', *Bulletin of Engineering Geology and the Environment*, vol. 83, no. 11, p. 478.